Editors' Suggestion

Signatures of Prethermalization in a Quenched Cavity-Mediated Long-Range Interacting Fermi Gas

Zemao Wu,[1] Jijie Fan,[1] Xue Zhang,[1] Jiansheng Qi,[1] and Haibin Wu[1,2,3,4,*]
[1]State Key Laboratory of Precision Spectroscopy, Institute of Quantum Science and Precision Measurement, East China Normal University, Shanghai 200062, China
[2]Shanghai Branch, Hefei National Laboratory, Shanghai 201315, China
[3]Collaborative Innovation Center of Extreme Optics, Shanxi University, Taiyuan 030006, China
[4]Shanghai Research Center for Quantum Sciences, Shanghai 201315, China

(Received 11 July 2023; revised 14 November 2023; accepted 16 November 2023; published 12 December 2023)

The coupling of ultracold quantum gases to an optical cavity provides an ideal system for studying the novel long-range interacting nonequilibrium dynamics. Here we report an experimental observation of the out-of-equilibrium dynamics of a degenerate Fermi gas in the cavity after quenching the pump strength over a superradiant quantum phase transition. The relaxation dynamics exhibits impressively different stages of a delay, violent relaxation, long-lifetime prethermalization, and slowly final thermalization due to the photon-mediated long-range interaction with dissipation. Importantly, we reveal that the lifetime of the system stayed on the prethermalization exhibits the superlinear scaling of the atom number. Furthermore, we show that the backaction of the superradiant cavity field on the gas causes the exchange of atoms between the normal and superradiant state in the early evolution and then induces the prethermalization. This work opens an avenue to explore complex nonequilibrium dynamics of the dissipatively long-range interacting Fermi gases.

DOI: 10.1103/PhysRevLett.131.243401

The long-range interaction is ubiquitous in many systems from the gravitationally bound globular clusters in astrophysics [1], two-dimensional incompressible fluid [2], and dipolar quantum gases [3] to heavy-ion collision in nuclear matter [4]. Understanding their dynamics is more challenging than those of the short-range interacting systems [5–8]. The nonadditivity of such long-range interacting systems exhibits many interesting out-of-equilibrium dynamics such as slow relaxation and broken ergodicity. One striking feature among these dynamics is that there exists a prethermalizing behavior associated with the emergence of a long-lifetime quasistationary state (QSS), before relaxing to the final steady state [5,6,8]. These dynamics are predicted in the isolated long-range systems under the deterministic Hamiltonian evolution [9]. The subsequent investigations show that the stochastic process and dissipation play important roles in the dynamical evolution, changing the time scales of the QSSs [9,10] and leading to the "scaling QSS" [11].

Coupling ultracold quantum gases to an optical cavity provides an ideal platform to study such phenomena with photon-mediated long-range interaction [12,13]. The superradiant quantum phase transition (SQPT), predicted for more than half a century [14,15], is realized by observing a self-ordering crystalline phase in the transversely driven Bose-Einstein condensates (BECs) [16,17]. Subsequently, the novel phenomena of combining the cavity quantum electrodynamics (QED) with ultracold bosonic atoms are investigated, such as a superradiant Mott insulator [18], dynamical phase transition [19], dissipative time crystal [20,21], and dissipation-engineered many-body dark states [22]. Recently, the coupling of Fermi gases and the cavity QED has been realized [23–25] and the fermionic SQPT has been observed [24].

Therefore, it is naturally expected to observe QSSs in such cavity-atom systems. Owing to the inevitable presence of dissipation via the leaking cavity field, these systems offer the unique opportunity to study such nonequilibrium dynamics with the driven-dissipative long-range interacting interactions. The mean-field calculation shows that the prethermalization emerges in the quenching dynamics of the cavity-mediated long-range interacting BEC system [26–28]. These studies found no evidence of the superlinear dependence of the QSS timescale on the atom number [5]. However, the observation of prethermalization and the QSS is still unexplored in the systems of either cavity bosonic or fermionic quantum gases.

In this Letter, we investigate the relaxation dynamics of an ultracold Fermi gas in the cavity after a sudden quench of the pumping strength across a driven-dissipative second-order phase transition. By transversely pumping the cavity, when the pumping power is adiabatically ramped over a critical value (threshold P_{th}), the intracavity field is abruptly built up and shows the steady-state SQPT where the Fermi gas experiences a self-ordering checkerboard pattern [Fig. 1(b)] [24]. Here, the pump power is suddenly

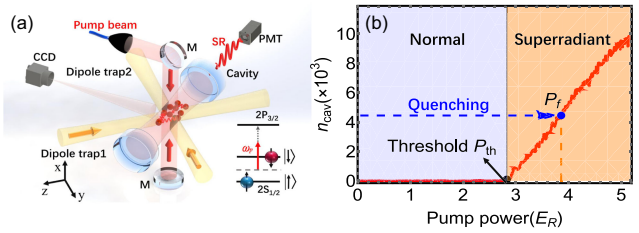

FIG. 1. (a) The schematics of experimental setup. Fabry-Perot cavity, high reflective mirror (M), photomultiplier (PMT), charge-coupled device (CCD). The frequency ω_c of the cavity is locked by a laser light at 1064 nm. The lower right corner is the energy levels. A laser light with frequency ω_p is red detuned by $2\pi \times 20$ GHz from the D_2 line of ^{6}Li to transversely pump atoms. (b) The mean intracavity photon numbers n_{cav} as a function of the pump power (red curve). When the pumping power is adiabatically ramped over a critical value (threshold P_{th}), the intracavity field is abruptly built up and shows a SQPT where atoms self-organized into a checkerboard pattern. Here, the pump-cavity detuning $\Delta \equiv (\omega_c - \omega_p) = -2\pi \times 900$ kHz, $T/T_F = 0.21(0.01)$ (T_F is the Fermi temperature), E_R is the recoil energy. A quench scenario is adopted by rapidly ramping the pump power over P_{th} to a final pump power P_f, which corresponds to quenching the system from a normal state to a superradiant (SR) state.

quenched to across P_{th} of the SQPT, and the system exhibits slow and complex relaxation dynamics that show several striking stages. After the quench, the cavity field is not instantaneously built up, experiences a long delay, and subsequently violently relaxes into a long-lifetime prethermalizing state due to the intracavity photon-mediated long-range interaction. After staying on the prethermalized state for several hundreds of the cavity lifetime, the cavity field further slowly evolves into its final nonequilibrium steady state. In experiments, the pump laser frequency is tuned far off resonance from the atom transition to ensure that the scattering processes are coherent and the dissipation is mainly from the inevitable leaking of the cavity field. The frequency detuning between the cavity resonant frequency and pump frequency is engineered to control the effective dissipation. Importantly, we investigate the scaling of the lifetime of the system that resides in the prethermalized states on the atom number, which clearly shows a superlinear relation. Our work may open an avenue to explore the novel many-body physics of the dissipative long-range interacting Fermi gases.

The experimental schematic is shown in Fig. 1, which is similar to our previous work [24]. A balanced mixture of ^{6}Li fermions is prepared in the two lowest hyperfine states $|\uparrow\rangle$ and $|\downarrow\rangle$, which is loaded into a crossed dipole trap to evaporatively cool to quantum degeneracy. The typical trapping frequencies of the optical potential are $(\omega_x, \omega_y, \omega_z)/2\pi = (290.69, 380.13, 84.97)$ Hz, where x, y, and z denote the pump axis, imaging axis, and cavity axis, respectively. The cavity is near confocal and has a finesse of $F = 1477$. The decay rate of the cavity field is $\kappa = 2\pi \times 677(36)$ kHz. The magnetically induced Feshbach resonance is used to tune the atom interaction into a noninteracting regime, resulting a typical temperature $T/T_F = 0.21(0.01)$, where $T_F = E_F/k_B$ is the Fermi temperature [$E_F = \hbar(\omega_x\omega_y\omega_z)^{1/3}(6N)^{1/3}$ is the Fermi energy], k_B is the Boltzmann constant, $\hbar$ is the Planck constant h divided by 2π, and N is the atom number per spin, respectively. An laser with frequency ω_p is red detuned about $2\pi \times 20$ GHz from the resonant frequency of the D_2 line of ^{6}Li to transversely pump the Fermi gas along the x axis. The frequency detuning Δ between the pump field and cavity resonant frequency ω_c is set as $\Delta = -2\pi \times 900$ kHz. The cavity field is monitored by a fast response high-gain photomultiplier. The spatial distribution of atoms is probed with an electron-enhanced charge-coupled device by using the standard resonant absorption imaging technique after a time-of-flight expansion time t_{tof}. When the pump power is increased over P_{th}, the cavity field is abruptly built and the atom fluctuations induce the SQPT [Fig. 1(b)]. The atoms at the momentum components $(p_x, p_z) = (\pm\hbar k_p, \pm\hbar k_p)$ spontaneously emerge and self-organize a checkerboard pattern [24].

Here, we adopt a quench scenario to explore nonequilibrium relaxation dynamics by rapidly turning on the pump field and quenching the system from the normal state to the superradiant state [see Fig. 1(b)]. The dynamics evolution of the intracavity field and atoms are detected in real time by monitoring the cavity transmission and imaging the atom distribution, respectively.

We investigate the time evolution of the cavity field by quenching the pumping power across the P_{th}. The pumping power is quenched from zero to the final pumping power P_f in a timescale less than 1 μs, then kept on the constant at P_f. The quenching dynamics of the cavity transmission is displayed for $P_f = 1.37P_{\mathrm{th}}$ in Fig. 2(a), which exhibits four distinct stages before reaching the final nonequilibrium steady state. After the pumping field is rapidly turned on, the cavity field is not instantaneously built up and there exists an impressive delay between the cavity field and pumping field at a timescale of several hundreds of the cavity lifetime (stage I). Subsequently, the evolution dynamics enters the second stage and the emergent cavity field experiences a violent relaxation process over the timescale of about tens of the cavity lifetimes (stage II). This relaxation stops at an intermediate value and then the cavity field shows a damped oscillation. After the oscillation is damped out, the cavity field stays a long-lifetime prethermalized state related to the so-called QSS (stage III). After remaining in this state for about several hundreds of the cavity lifetime, the cavity field slowly grows to the final nonequilibrium stationary state on a much longer timescale, about 3 orders of magnitude of the cavity lifetime (stage IV). The numerical simulation of the dynamics including more momentum states for the Fermi gas qualitatively agrees with the experimental observation and clearly shows

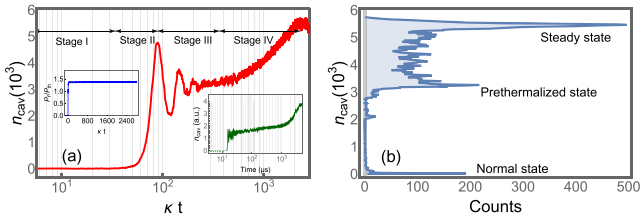

FIG. 2. The relaxation dynamics of quenching the pump power over $P_{\rm th}$ of the SQPT to the final pump power P_f. (a) A typical trajectory of the mean intracavity photon numbers $n_{\rm cav}$ for quenching dynamics with different stages (red curve). The parameters are $\kappa = 2\pi \times 677(36)$ kHz, $\Delta = -2\pi \times 900$ kHz and $T/T_F = 0.21(0.01)$, respectively. Insets show that the pump power is suddenly turned on from 0 to $P_f/P_{\rm th} = 1.37$ (blue curve) and the numerical simulation (green curve), respectively. (b) The histogram of the cavity transmission. Three peaks are clearly shown, which refer to the normal state, prethermalized state, and the steady state, respectively.

these stages in the evolution [inset in Fig. 2(a), see the Supplemental Material [29]]. Figure 2(b) shows the histogram of the cavity transmission with a bin of 3.67 μs $(15.6/\kappa)$. It clearly shows that the relaxation dynamics exhibits three characteristic states in the evolution: one normal state and two superradiant states. The first peak represents the fact that the Fermi gas stays in the normal state where no cavity light is observed. The second one represents the prethermalized state, and the third denotes that the system enters the final nonequilibrium steady state.

At stage I, the system stays in the normal state and there is a delay between the buildup of the cavity field and pumping field. It is commonly considered that this delay arises as a result of the quantum description of dynamics of the Dicke state [30] and has been recently investigated in pulsed superradiant lasing with bosonic atoms [31]. The delay time is dependent on the quenching pump power and the number of atoms. $\tau_d/t_{\rm cav}$ as a function of $P_f/P_{\rm th}$ is displayed in Fig. 3, where τ_d is the delay time and $t_{\rm cav} = 1/(2\kappa)$ is the lifetime of the cavity intensity, respectively. It is clearly shown that the closer the quenching pump power P_f is to the threshold $P_{\rm th}$, the longer is the delay time. When the quenching pump power is very near to the threshold of the phase transition, a critical slowing is expected and the delay time τ_d could be several thousands of $t_{\rm cav}$. The prethermalization is almost difficult to be observed under this condition and even disappears, as shown in the inset of Fig. 3(a), where $P_f/P_{\rm th} = 1.08$. For the large $P_f/P_{\rm th}$, the delay time quickly becomes small. Over $P_f/P_{\rm th} = 1.2$, τ_d approaches a fixed value of around $2h/E_R$.

After the delay, the cavity field begins to rapidly build up and experiences the violent relaxation in stage II. With the increase of the cavity field, atoms that felt optical potential consisted of the pumping field and the emergent intracavity field. Therefore, atoms self-organized into

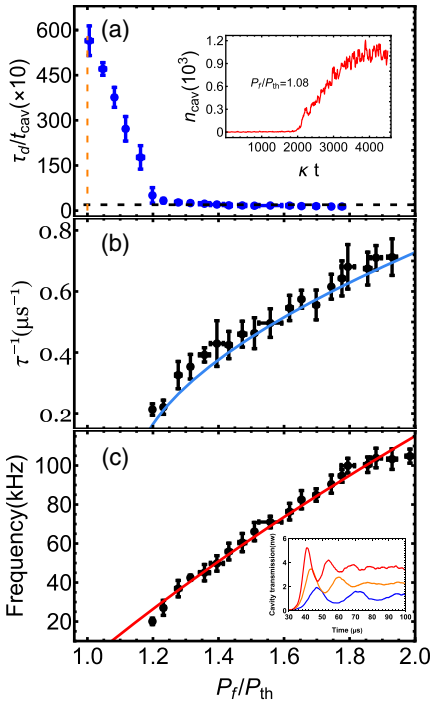

FIG. 3. (a) The dependence of the delay time τ_d on $P_f/P_{\rm th}$. τ_d is approached to a fixed value of around $2h/E_R$ (dashed horizontal line) when $P_f/P_{\rm th} > 1.2$. Inset: time evolution of the cavity transmission when quenching pump power is close to the threshold, $P_f/P_{\rm th} = 1.08$. (b) The characteristic growth rate τ^{-1} as a function of $P_f/P_{\rm th}$, where τ is obtained from an exponential function fit of $A\exp(t/\tau) + B$ for the violent relaxation dynamics. The solid line is a quadratic fit to guide the eye. (c) The dependence of the oscillated frequencies on $P_f/P_{\rm th}$ in stage III. Inset: the oscillated dynamics of the cavity transmission for $P_f/P_{\rm th} = 1.31$ (blue curve), $P_f/P_{\rm th} = 1.47$ (orange curve), and $P_f/P_{\rm th} = 1.65$ (red curve), respectively, which clearly show the oscillations and following prethermalization. The red solid curve is the fit with a function of $c_1 P^{1/2} + f_0$. Error bars represent the standard statistical deviation.

higher momentum states. The growth of the cavity field in this stage can be well fitted by an exponentially increasing function $A\exp(t/\tau) + B$. The characteristic growth rate τ^{-1} as a function of $P_f/P_{\rm th}$ is presented in Fig. 3(b). As the quenching pump power increases, the relaxation dynamics of the cavity field becomes more violent. After the stage of the violent relaxation, the cavity transmission oscillates around the intermediate value as shown in Fig. 2(a). The energy of the atom is periodically transferred from the kinetic to the potential energy. With the large quenching pump power, the oscillated frequencies become large [Fig. 3(c)]. The oscillation is involved in a process involving the absorption and emission of cavity (pump) photon [see the third term of Eq. (2) in the Supplemental Material [29]]. Therefore, oscillated frequencies obey a scaling of $P^{1/2}$ [red solid curve in Fig. 3(c)]. Subsequently, the evolution dynamics of the

cavity field exhibits the prethermalization after the oscillation has died out. The interplay between long-range conservative and dissipative forces results in the emergence of the prethermalization [27], which is closely related to quantum statistics (see the Supplemental Material [29]). After the prethermalization stage, the cavity transmission slowly grows to the stationary value over timescales of 3 orders of magnitude of the cavity lifetime.

We investigate the lifetime of the system trapped in the prethermalized state. It has been well accepted that the long-range interacting system could quickly relax to the QSS in the nonequilibrium dynamics. A prototype model of the long-range interaction, the Hamiltonian mean-field model, has shown that the system remains trapped in the QSS for times that increase with a nontrivial scaling of the atom number as $N^{1.7}$ [32,33] and the lifetime of the QSS diverges when the atom number increases in the thermodynamical limit; however, no such feature was found in the recent study for the BEC in the cavity [26]. For Fermi gases, the fermionic statistics causes a qualitatively different self-ordering behavior [34–36] compared to bosons. Correspondingly, the Fermi energy would play an important role in the quenching dynamics [37]. The simple numerical calculation shows that the quantum statistics profoundly affects the lifetime of the prethermalization (see the Supplemental Material [29]). In the experiment, the scaling of the lifetime τ_p of the system in the prethermalized state on the atom number N is investigated, as shown in Fig. 4. We vary the number N of atoms and keep T/T_F nearly constant by precisely controlling the evaporative cooling process (inset of Fig. 4). The Pauli exclusion principle causes the threshold P_{th} of the fermionic SQPT to have a scaling of $N^{-1/2}$ at a low temperature [24]. Therefore, the final quench pump power is set at $P_f = 1.3P_{\mathrm{th}}$ for the maximum available atom numbers of about 150 000. As shown in Fig. 4, the scaling clearly exhibits the different behavior for N. For the smaller N, the lifetimes τ_p become longer as N increases and, importantly, the scaling of τ_p shows a superlinear relation on N. The fit of the data with a simple function $\tau_p = cN^s + \tau_0$ gives the scaling $s = 1.53(1.1)$ for N from 80 000 to 110 000 (red dashing line in Fig. 4), which is close to the theoretical predictions $s = 1.7$ [33]. However, this relation breaks down (τ_p becomes to deviate this scaling at $N \approx 12\,000$) and τ_p shows the sign of saturating for large N. By continuing to increase N, the lifetime τ_p of the system in the prethermalized state shows a trend of decrease, which may likely be caused by the fact that more momentum states in the superradiant states are occupied and the scattering probability is decreased for the very large atom number.

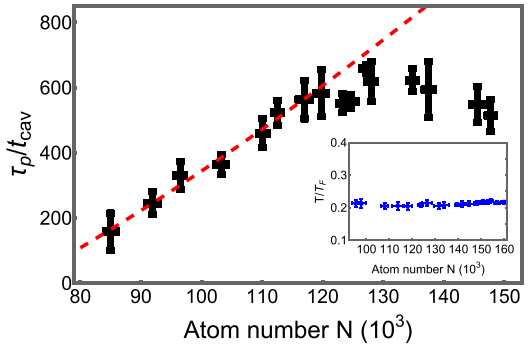

FIG. 4. The lifetimes τ_p of the system remained on the prethermalization as a function of the atom number N at the low temperature of $T/T_F = 0.21(0.01)$ for a fixed quenching pump power of $P_f = 1.3P_{\mathrm{th}}$, where $\Delta = -2\pi \times 900$ kHz. The dashed line is a fit with the function of $\tau_p = cN^s + \tau_0$, which gives $s = 1.53(1.1)$. Inset: the dimensionless temperature T/T_F as a function of the atom number N.

We also study the quenching dynamic evolution of the self-organization of fermionic superradiance by measuring the atom fraction at different momentum states. After the quench, the emergent superradiant cavity field scattering from the atoms puts a backaction on the Fermi gas, for which the dynamics of atoms in momentum space exhibits new features, as displayed in Fig. 5. Before the SQPT, atoms are mainly distributed around the momentum states P_b of $|p_x, p_z\rangle = |0, 0\rangle$, $|\pm 2\hbar k_p, 0\rangle$, and $|0, \pm 2\hbar k_p\rangle$. After the SQPT, the interference between the cavity field and pumping lattice causes the emergent checkerboard pattern

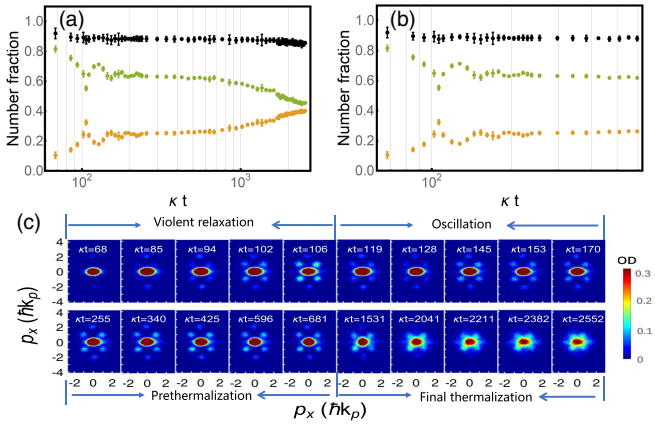

FIG. 5. Dynamical evolution of the atom distribution. (a) Atom number fraction (normalized to the total atom number) for the different momenta as a function of evolution time. Green dots are the atom number fraction corresponding to the momentum ranges $(p_x, p_z) = [\pm(-0.5 - 0.5), \pm(-0.5 - 0.5)]\hbar k_p$ and $[\pm(-1.5 - 2.5), \pm(-1.5 - 2.5)]\hbar k_p$. Orange dots are the atom number fraction corresponding to the momentum ranges $(p_x, p_z) = [\pm(0.5 - 1.5), \pm(0.5 - 1.5)]\hbar k_p$. Black dots are the summation of atoms for these momentum states. Error bars represent the standard deviation of five measurements. (b) The closer inspections of the dynamics evolution at $\kappa t \sim 60$–600. It shows an exchange of atoms between different momentum states and the emergence of the prethermalization after the violent relaxation. (c) The dynamical evolution of the atom density distribution with $t_{\mathrm{tof}} = 1300$ μs. The other parameters are the same as Fig. 2.

of atoms, where atoms are piled around the momentum states P_a of $|p_x, p_z\rangle = |\pm\hbar k_p, \pm\hbar k_p\rangle$. Green and oranges dots in Fig. 5(a) show the fraction of atoms around the momentum states P_b and P_a, respectively. After the quench, waiting for several hundreds of the cavity lifetime, atoms in momentum states of P_b are rapidly decreased and more atoms are excited into the momentum states around P_a. Strikingly, after such the initial violent relaxation, atoms are oscillated back and forth between the momentum states around P_b and P_a and subsequently enter into a prethermalized state [Fig. 5(b)]. The atoms stay in the state for hundreds of microseconds and then slowly evolve into their final nonequilibrium states. Figure 5(c) shows evolution of the atom density distribution with a $t_{\mathrm{tof}} = 1300$ μs, which clearly shows the initially violent relaxation, oscillation, prethermalization, and long-time slow relaxation of the atom fraction in different states, respectively. The long-time dynamical behavior of atoms is similar to the expansion of the Fermi gas in the lattice [38].

In conclusion, we have studied the quenching dynamics of the harmonically trapped ultracold Fermi gas in the optical cavity. When the pump strength is quenched over the phase transition of the driven-dissipative SQPT, the observed slow relaxation dynamics shows the strikingly different stages. Both the cavity field and atoms exhibited the long-lifetime prethermalization. The superlinear scaling of the lifetime of the system remained on the prethermalization with the atom number revealed. Our Letter will open the possibilities to study novel nonequilibrium with long-range interactions, such as dynamical gauge coupling [39], manipulating the intertwined orders [40], Higgs mode stabilization [41], and many-body localizations [42].

We thank G. Morigi, C. Zhang, and H. Zhai for helpful discussions. This research is supported by the National Key Research and Development Program of China (Grant No. 2022YFA1404202), National Natural Science Foundation of China (NSFC) (Grants No. 11925401, No. 12234008, No. 12074125), Innovation Program for Quantum Science and Technology (ZD0202090201), and the Shanghai Municipal Science and Technology Major Project (No. 2019SHZDZX01).

*hbwu@phy.ecnu.edu.cn

[1] T. Padmanabhan, Phys. Rep. **188**, 285 (1990).
[2] J. Miller, Phys. Rev. Lett. **65**, 2137 (1990).
[3] N. Defenu, T. Donner, T. Macrì, G. Pagano, S. Ruffo, and A. Trombettoni, Rev. Mod. Phys. **95**, 035002 (2023).
[4] S. Huth, P. T. H. Pang, I. Tews, T. Dietrich, A. Le Fèvre, A. Schwen, W. Trautmann, K. Agarwal, M. Bulla, M. W. Coughlin, and C. Broeck, Nature (London) **606**, 276 (2022).
[5] A. Campa, T. Dauxois, and S. Ruffo, Phys. Rep. **480**, 57 (2009).
[6] I. Latella, A. Pérez-Madrid, A. Campa, L. Casetti, and S. Ruffo, Phys. Rev. Lett. **114**, 230601 (2015).
[7] F. Bouchet, S. Gupta, and D. Mukamel, Physica (Amsterdam) **389A**, 4389 (2010).
[8] A. Polkovnikov, K. Sengupta, A. Silva, and M. Vengalattore, Rev. Mod. Phys. **83**, 863 (2011).
[9] S. Gupta and D. Mukamel, Phys. Rev. Lett. **105**, 040602 (2010).
[10] C. Nardini, S. Gupta, S. Ruffo, T. Dauxois, and F. Bouchet, J. Stat. Mech. (2012) P12010.
[11] M. Joyce, J. Morand, F. Sicard, and P. Viot, Phys. Rev. Lett. **112**, 070602 (2014); M. Joyce and T. Worrakitpoonpon, Phys. Rev. E **84**, 011139 (2011); M. Joyce, J. Morand, and P. Viot, Phys. Rev. E **93**, 052129 (2016).
[12] H. Ritsch, P. Domokos, F. Brennecke, and T. Esslinger, Rev. Mod. Phys. **85**, 553 (2013).
[13] F. Mivehvar, F. Piazza, T. Donner, and H. Ritsch, Adv. Phys. **70**, 1 (2021).
[14] R. H. Dicke, Phys. Rev. **93**, 99 (1954).
[15] K. Hepp and E. H. Lieb, Ann. Phys. (N.Y.) **76**, 360 (1973); Y. K. Wang and S. T. Hioe, Phys. Rev. A **7**, 831 (1973).
[16] K. Baumann, C. Guerlin, F. Brennecke, and T. Esslinger, Nature (London) **464**, 1301 (2010).
[17] D. Nagy, G. Kónya, G. Szirmai, and P. Domokos, Phys. Rev. Lett. **104**, 130401 (2010).
[18] J. Klinder, H. Keßler, M. R. Bakhtiari, M. Thorwart, and A. Hemmerich, Phys. Rev. Lett. **115**, 230403 (2015).
[19] J. Klinder, H. Keßler, M. Wolke, L. Mathey, and A. Hemmerich, Proc. Natl. Acad. Sci. U.S.A. **112**, 3290 (2015).
[20] H. Keßler, J. G. Cosme, M. Hemmerling, L. Mathey, and A. Hemmerich, Phys. Rev. A **99**, 053605 (2019).
[21] H. Keßler, P. Kongkhambut, C. Georges, L. Mathey, J. G. Cosme, and A. Hemmerich, Phys. Rev. Lett. **127**, 043602 (2021).
[22] R. Lin, R. Rosa-Medina, F. Ferri, F. Finger, K. Kroeger, T. Donner, T. Esslinger, and R. Chitra, Phys. Rev. Lett. **128**, 153601 (2022).
[23] K. Roux, H. Konishi, V. Helson, and J.-P. Brantut, Nat. Commun. **11**, 2974 (2020).
[24] X. Zhang, Y. Chen, Z. Wu, J. Wang, J. Fan, S. Deng, and H. Wu, Science **373**, 1359 (2021).
[25] H. Konishi, K. Roux, V. Helson, and J. P. Brantut, Nature (London) **596**, 509 (2021).
[26] S. Schütz and G. Morigi, Phys. Rev. Lett. **113**, 203002 (2014).
[27] S. Schutz, S. B. Jager, and G. Morigi, Phys. Rev. Lett. **117**, 083001 (2016).
[28] S. Schütz, S. B. Jäger, and G. Morigi, Phys. Rev. A **92**, 063808 (2015).
[29] See Supplemental Material at http://link.aps.org/supplemental/10.1103/PhysRevLett.131.243401 for mean field approximation and simulations including quantum statistic, and the experimental measurement of the atom number scaling of the prethermalization and steady states.
[30] M. Gross and S. Haroche, Phys. Rep. **93**, 301 (1982).
[31] T. Laske, H. Winter, and A. Hemmerich, Phys. Rev. Lett. **123**, 103601 (2019).
[32] Y. Y. Yamaguchi, Phys. Rev. E **68**, 066210 (2003).
[33] Y. Y. Yamaguchi, J. Barre, F. Bouchet, T. Dauxois, and S. Ruffo, Physica (Amsterdam) **337A**, 36 (2004).
[34] J. Keeling, M. J. Bhaseen, and B. D. Simons, Phys. Rev. Lett. **112**, 143002 (2014).

[35] F. Piazza and P. Strack, Phys. Rev. Lett. **112**, 143003 (2014).
[36] Y. Chen, Z. Yu, and H. Zhai, Phys. Rev. Lett. **112**, 143004 (2014).
[37] R. M. Sandner, W. Niedenzu, F. Piazza, and H. Ritsch, Europhys. Lett. **111**, 53001 (2015).
[38] U. Schneider, L. Hackermüller, J. P. Ronzheimer, S. Will, S. Braun, T. Best, I. Bloch, E. Demler, S. Mandt, D. Rasch, and A. Rosch, Nat. Phys. **8**, 213 (2012).
[39] W. Zheng and N. R. Cooper, Phys. Rev. Lett. **117**, 175302 (2016).
[40] J. Li and M. Eckstein, Phys. Rev. Lett. **125**, 217402 (2020).
[41] H. Gao, F. Schlawin, and D. Jaksch, Phys. Rev. B **104**, L140503 (2021).
[42] P. Sierant, K. Biedron, G. Morigi, and J. Zakrzewski, SciPost Phys. **7**, 008 (2019).